

SPECTRAL PROPERTIES OF SHUNGITE QUANTUM DOTS

B. S. Razbirin¹, N. N. Rozhkova², E. F. Sheka³,
D. K. Nelson¹, A. N. Starukhin¹, A. S. Goryunov⁴

¹Ioffe Physical-Technical Institute, RAS, Saint Petersburg, Russia

²Institute of Geology Karelian Research Centre RAS, Petrozavodsk, Russia

³Peoples' Friendship University of Russia, Moscow, Russia

⁴Institute of Biology Karelian Research Centre RAS, Petrozavodsk, Russia

³sheka@icp.ac.ru

PACS 73.63.Kv, 73.23.Hk, 73.43.Lp, 78.67.Wj

A low-temperature study has been performed for aqueous shungite, carbon tetrachloride, and toluene dispersions. Spectral characteristics for graphene quantum dots (GQDs) of shungite, attributed to individual fragments of reduced graphene oxide (rGO), reveal a dual character of the dispersions emitting centers: individual GQDs are responsible for the spectra position while fractal structure of GQD colloids provides large broadening of the spectra due to structural inhomogeneity of the colloidal dispersions and a peculiar dependence of photoluminescence of dispersions on excitation wavelength. For the first time, photoluminescence spectra of individual GQDs were observed in frozen toluene dispersions, which pave the way for a theoretical treatment of GQDs photonics.

Keywords: graphene quantum dots, fractals, photoluminescence, colloidal dispersions, shungite.

1. Introduction

The fractal structure of shungite promotes the formation of its water dispersions, for which homogeneity can be achieved by sonication and filtration. The dispersions present colloidal aggregates of nanosize fragments of reduced graphene oxide (rGO) of ~ 1 nm in size dissolved in water. These pristine fragments are attributed to graphene quantum dots (GQDs) of shungite [1]. The spectral study presented in the current paper was aimed at revealing a similarity in spectral behavior for GQDs of shungite and synthetic GQDs, thus confirming the grounds for the fractal structure of shungite.

Originally, the term 'graphene quantum dot' (GQD) appeared in theoretical research and was attributed to fragments limited in size, or domains, of a single-layer two-dimensional graphene crystal. The subject of these investigations concerned quantum size effects, manifested in the spin [2,3], electronic [4] and optical [5–10] properties of the fragments. The latter study significantly stimulated the interest in GQDs, so that the question arose of their preparation. This proved to be a difficult task, and the progress achieved to this point has been presented in exhaustive reviews [11,12]. Spectral studies have found that in almost all cases, GQDs are not single-layer graphene domains, but multi-layer formations containing up to 10 layers of reduced graphene oxide (rGO) from 10 to 60 nm in size. However, to obtain single-layer GQDs is also not uncommon (see, for example [13–17]).

Optical spectroscopy, specifically photoluminescence (PL), is the primary method for studying the properties of the GQDs. The review [12] presents an exhaustive complete picture of the results. As was shown, optical spectroscopy of GQDs gives a complicated picture with many features. However, in spite of this diversity, common patterns can be identified that can serve as a basis for spectral analysis of the GQDs. These general characteristics include:

1) structural inhomogeneity of GQDs solutions, better called dispersions; 2) low concentration limit that provides surveillance of the PL spectra; 3) dependence of the GQD PL spectrum on the solvent, and 4) dependence of the GQD PL spectrum on the excitation light wavelength. These four circumstances determine the usual conditions under which the spectral analysis of complex polyatomic molecules is performed. Optimization of conditions, including, primarily, the choice of solvent and the experiment performance at low temperature, in many cases, led to good results, based on structural PL spectra (see, for example, the relevant research of fullerenes solutions [18–21]). In this paper, we will show that implementation of this optimization for spectral analysis of the GQDs turns out to be quite successful.

2. Fractal Nature of the Object under Study

A concept on GQD evidently implies a dispersed state of a number of nanosize rGO fragments. Empirically, the state is provided by the fragments' dissolution in a solvent. Once dissolved, the fragments unavoidably aggregate, forming colloidal dispersions. As mentioned earlier, so far only aqueous dispersions of synthetic GQDs have been studied [11, 12]. In the case of shungite GQDs, two above-mentioned organic solvents were used when replacing water in the pristine dispersions. In each of these cases, the colloidal aggregates are the main object of the study. In spite of that, so far, there has not been any direct confirmation of their fractal structure, there are serious reasons to suppose that this is an obvious reality. Actually, first, the rGO fragments formation occurred under conditions that unavoidably involve elements of randomness during both laboratory chemical reactions and natural graphitization [1]; the latter concerns the fragments' size and shape. Second, the fragments' structure certainly bears the stamp of polymers, for which fractal structure of aggregates in dilute dispersions has been convincingly proven (see [22] and references therein).

As shown in [22], the fractal structure of colloidal aggregates is highly sensitive to the solvent around, the temperature of the aggregate formation, as well as other external factors such as mechanical stress and so forth. This fact makes the definition of quantum dots of colloidal dispersions at the structural level quite undefined. In the case of the GQDs of different origin, the situation is additionally complicated, since the aggregation of synthetic (Sy) and natural shungite (Sh) rGO fragments occurred under different external conditions. In view of this, it must be assumed that not only rGO-Sy and rGO-Sh aggregates, but the same solvent dispersions are quite different.

Looking for the answer to the question if the same term GQD can be attributed to colloidal dispersion in the above two cases, one should recall that a feature of fractal structures is that fractals are typically self-similar patterns, where 'self-similar' means that they are 'the same from near as from far' [23]. This means that the peculiarities of, say, optical behavior for both rGO-Sy and rGO-Sh colloidal dispersions obey the same law. From this viewpoint, there is apparently no difference for which the structural element of a multilevel fractal structure of their colloidal aggregates should be attributed to a quantum dot. However, the identity of both final and intermediate fractal structures of aggregates in different solvents is highly questionable and only the basic rGO structural units cast no doubts. Because of this, GQDs of both rGO-Sy and rGO-Sh dispersions should be associated with rGO individual fragments. Therefore, different fractal nets of GQDs provided by different colloidal dispersions present the object under the current study. Addressing the spectral behavior of the dispersions, we should expect an obvious generality provided by the common nature of GQDs, but simultaneously complicated by the difference in fractal packing of the dots in the different-solvent dispersions. The current study provides confirmation for this vision of spectral behavior on an example of rGO-Sh dispersions.

3. Experimental Techniques

Morphological investigation of rGO-Sh dispersions concerned defining the size distribution of the dispersions' colloidal aggregates and obtaining overview pictures of the structure of films obtained therein by evaporation of the solvent. The relevant size-distribution profiles were obtained using dynamic light scattering incorporated in nanoparticle size analyzer Zetasizer Nano ZS (Malvern Instruments). Processing of the results was carried out using a spherical shape approximation for the aggregates. Spectral studies were carried out at 293 K and 80 K. Emission spectra of liquid and frozen dispersions were excited by laser lines λ_{exc} of 337.1, 405, 457, 476.5, 496.5, 514.5 and 532 nm. The resulting spectra were normalized to the power of the laser radiation at different excitations. The spectra were recorded under identical conditions on a DFS-12 spectrometer with a spectral resolution ≈ 0.2 nm. The obtained data are related to shungite of 98 wt.% carbon.

4. Aqueous Dispersions

In full agreement with commonly used methods [24, 25], rGO-Sh aqueous dispersions were obtained by sonication of the pristine shungite powder for 15 min with an ultrasonic disperser US-2M (at a frequency of 22 kHz and the operating power 300 W) at 300 °C followed by filtration and ultracentrifugation [26]. The maximum achievable concentration of carbon is less than 0.1 mg/ml, which is consistent with poor water solubility of graphene and its derivatives [24]. The resulting dispersions are quite stable, and their properties vary little over time. The size-distribution characteristic profile of rGO-Sh aggregates is shown in Fig. 1a. The average size of the aggregates is 54 nm, its full width at half maximum constitutes 26 nm so that the resulting colloids are significantly inhomogeneous. The inhomogeneity obviously concerns both the size and shape (and, consequently, chemical composition) of basic rGO fragments, and thus GQDs. The structure of the carbon condensate formed after water evaporation from the dispersion droplets on a glass substrate is shown in Fig. 1b and 1c. As seen from the figure, the condensate is of a fractal structure formed by ball-like aggregates. It should be mentioned that the condensate's fractal structure should not be identical to that one of the pristine dispersion [22], although, no doubt, some continuity of the structure should take place.

Figure 2a shows an overview of the characteristic patterns for the emission spectrum of rGO-Sh aqueous dispersions at different excitation lines. Increasing the temperature to 293 K did not cause a significant change in the spectra, resulting in only a slight broadening of their structural component related to the Raman spectrum of water at the O–H stretching vibrations of ~ 3400 cm^{-1} . When excited at λ_{exc} 405 and 457 nm, Raman spectrum superimposes the broad luminescence band in the 17000 – 22000 cm^{-1} region. The emission of the dispersion at λ_{exc} 532 nm is weak. Fig. 2b shows the PL spectra of the aqueous dispersion at λ_{exc} 405 and 457 nm after subtraction of the Raman spectra of water. Both spectra present broad bands characteristic of the PL spectra for rGO-Sy aqueous dispersions (see [12]). In spite of the large width of PL spectra, their position in the same spectral region for both rGO-Sy and rGO-Sh aqueous dispersions gives evidence for a common nature of emitting GQDs.

The similarity of the spectral behavior for the two dispersions also involves a considerable overlapping of their absorption and PL spectra, so that a set of new PL spectra can be excited with an increase λ_{exc} . Of course, a shift of these new PL spectra maxima towards longer wavelengths with increasing λ_{exc} is observed. Such behavior usually indicates the presence of an inhomogeneously broadened absorption spectrum of the emitter, which widely overlap with PL one and whose excitation at different λ_{exc} within the overlapping region results in selective

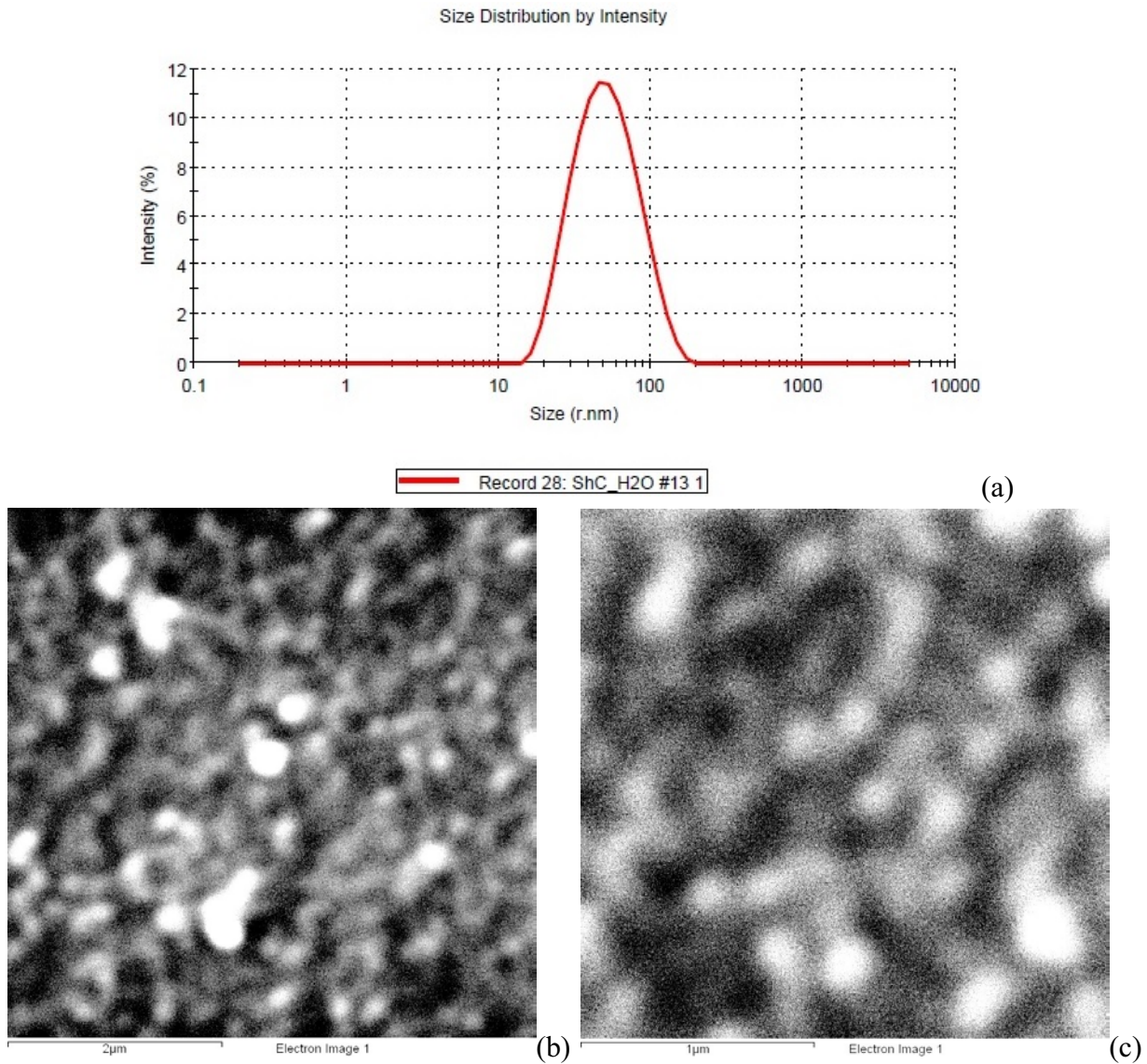


FIG. 1. Size-distribution profile of colloidal aggregates in shungite water dispersion (a) and SEM images of the dispersion condensate on glass substrate (b) and (c): Scale bar $2 \mu\text{m}$ and $1 \mu\text{m}$, respectively. Carbon concentrations constitute 0.1 mg/ml

excitation of different sets of emitting centers. In the case of rGO-Sy dispersions, the inhomogeneous broadening of the spectra is usually explained by scatter in the GQDs (rGO fragments) linear dimensions [12]. However, not only GQDs linear dimensions, but their shape as well as the composition of colloidal aggregates may largely vary, which should be expected for the rGO-Sh dispersions, in particular. This is clearly seen on the example of various aggregates structure of the condensates shown in Fig. 1b and 1c. Unfortunately, the large width of the PL spectra does not allow one to exhibit those spectral details that might speak about aggregated structure of GQDs.

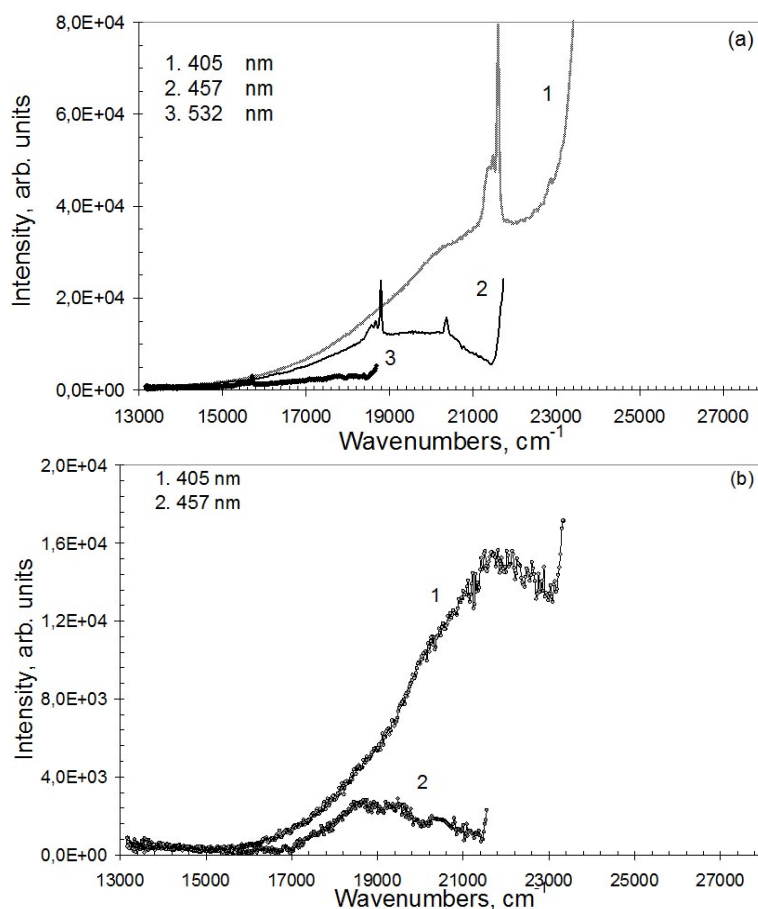


FIG. 2. Photoluminescence spectra of shungite water dispersions at 80 K as observed (a) and after subtraction of Raman scattering of water (b). Figures mark excitation wavelengths

5. Dispersions in Organic Solvents

Traditionally, the best way to overcome difficulties caused by inhomogeneous broadening of optical spectra of complex molecules is the use of their solutions in specially selected crystalline matrices. Carbon tetrachloride and toluene are known to provide a reliable monitoring of fine-structured spectra for individual molecules (Shpol'skii's effect [27]) as it was, say, in the case of fullerenes [18–21]. Detection of PL structural spectra or structural components of broad PL spectra not only simplify spectral analysis, but indicate the dispersing of emitting centers of complex structure into individual molecules. It is this fact that was the basis for the solvent choice when studying spectral properties of shungite GQDs.

Organic rGO-Sh dispersions were prepared from the pristine aqueous dispersions during sequential replacement of water by isopropyl alcohol first and then by carbon tetrachloride or toluene [26]. The morphology and spectral properties of these dispersions turned out to be quite different.

5.1. Dispersions in Carbon Tetrachloride

When analyzing CTC-dispersion morphology, the first important discovery was that a drastic change in the size-distribution profiles occurs for the dispersion aggregates in comparison with those of the aqueous dispersions (see Fig. 3). This finding gives direct evidence for the

fractal nature of the GQDs aggregates in water, since only under these conditions can such a strong effect, caused by solvent substitution, be observed [22]. The second result concerns the high uncertainty in this fractal structure. Thus, Figs. 3a and 3b present size-distribution profiles related to CTC-dispersions, which were most different from this viewpoint. Figs. 3c and 3d show images of film agglomerates obtained when drying the CTC-dispersion droplets on glass. As can be seen by comparing Fig. 1 and Fig. 3, the average colloidal aggregate size drastically increases when water is substituted with carbon tetrachloride. Simultaneously, the scatter of sizes increases that is comparable with the size itself in the limiting case. The nearly spherical shape of aggregates in Figs. 1b and 1c is replaced by lamellar faceting, mostly characteristic of microcrystals. The absence of small aggregates is noteworthy, which indicates a complete absence of individual GQDs in the dispersions. Therefore, the change in size-distribution profiles as well as in shape of the aggregates of the condensate points to a strong influence of solvent on the aggregates' structure, thus decisively confirming their fractal character.

The conducted spectral studies are very consistent with these findings. Fig. 4 shows PL spectra of CTC-dispersion DC1, morphological properties of which are near to those shown in Fig. 3a. The dispersions have a faint yellow-brown color, which indicates the presence of significant absorption of the solutions in the visible region (see Fig. 4a). PL spectra were studied for a wide range of dispersions obtained at different times. As found both these spectra behavior at different exciting lasers λ_{exc} and the PL spectra shape of different dispersions are largely similar, while the spectral intensity can differ substantially. Arrows in Fig. 4a show wave number values λ_{exc}^{-1} corresponding to laser lines at 405, 457, 476.5, 496.5, 514.5 and 532 nm. As can be seen in Fig. 4a, the dispersion absorption increases when advancing to the UV region. It can be assumed that the absorption of each component of the aggregates' conglomerate increases with decreasing λ_{exc} , so that the excitation with UV light at $\lambda_{exc} = 337.1$ nm affects almost all luminescence centers in the crystal matrix. Actually, the UV excited PL spectrum in Fig. 4a is very broad and covers the region from 27000 to 15000 cm^{-1} . In this case, the PL spectrum overlaps with the absorption spectrum over the entire spectral range. Such a large overlapping gives evidence for the inhomogeneously broadened character of both spectra that is, the formation of an ensemble of emitting centers, which differ in the probability of emission (absorption) at given wavelength. Actually, successive PL excitation by laser lines 1, 3, 4 and 5 (see Fig. 4a) causes a significant modification of the PL spectra (Fig. 4b). The width of the spectra decreases as λ_{exc} increases, the PL band maximum is shifted to longer wavelengths, and the spectrum intensity decreases. This is due to selective excitation of a certain group of centers. In general, the observed pattern is typical for structurally disordered systems discussed in the previous section. To simplify further comparative analysis of the spectra obtained at different λ_{exc} , we shall denote them according to the excitation wavelength, namely: 405-, 476-, 496-spectrum, etc.

Comparing the PL spectra of dispersion DC1 at different excitations, we note that 1) PL spectra, obtained when excited in the region of overlapping absorption and emission spectra in Fig. 4a, have a more distinct structure than the 337-one but still display a superpositioning character of the spectra; 2) the intensity of the 405-spectrum is almost an order of magnitude higher than the intensity of the rest of the spectra. Before discussing the observed spectral features, let us look at the PL spectra of dispersion DC2 that is close in morphology to the dispersion shown in Fig. 3b. Fig. 5a compares the 337- and 405- spectra of DC2 with those of DC1 described earlier. The 337-spectrum of DC2 exhibits a new UV band, intensity of its 405-spectrum decreases by several times. The spectrum of DC2 still retains a three-peak shape, but their intensities are significantly redistributed. This evidently refers to the superpositioning

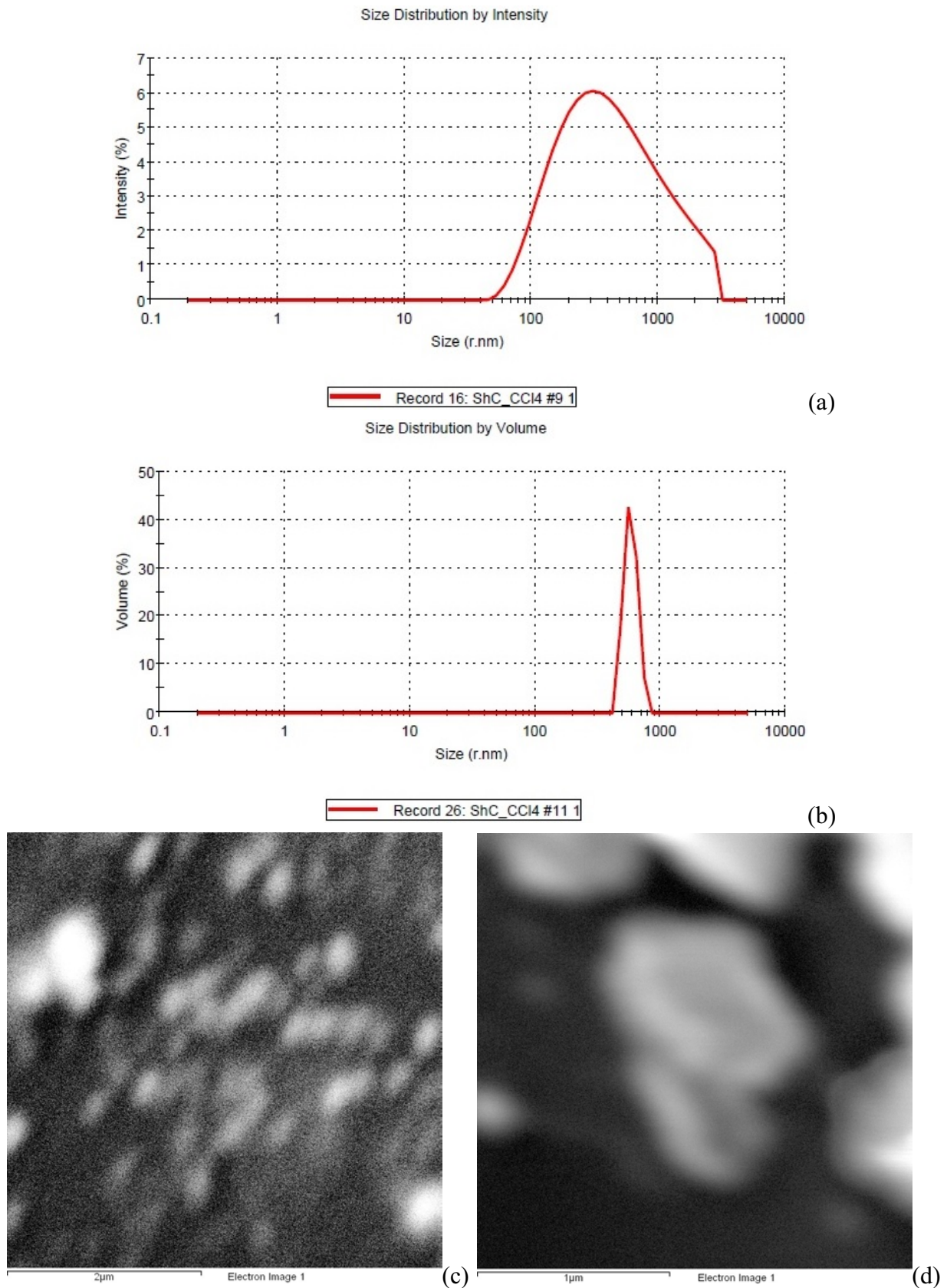


FIG. 3. Size-distribution profiles of colloidal aggregates in shungite dispersion in carbon tetrachloride (a and b) (see text) and SEM images of the dispersion condensates on glass substrate (c) and (d): Scale bar $2 \mu\text{m}$ and $1 \mu\text{m}$, respectively

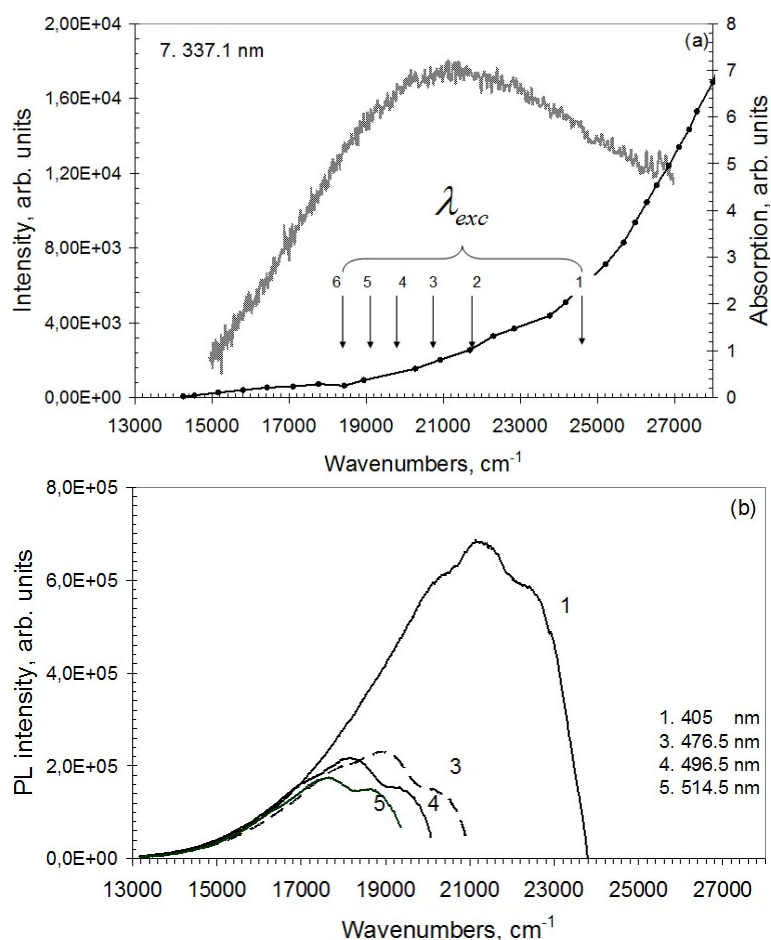


FIG. 4. Photoluminescence (a and b) and absorption (a) spectra of shungite dispersion in carbon tetrachloride DC1 at 80 K after background emission subtraction. Figures mark excitation wavelengths

character of the spectrum as said before. It is important to note that the 405-spectrum of DC2 is still the most intense among other DCQ spectra (see Fig. 5b).

Comparative analysis of the PL spectra of dispersions DC1 and DC2 shows that the above-mentioned spectral regularities are sensitive to the CTC-dispersion's structure and are directly related to the degree of structural inhomogeneity. Thus, the narrowing of the size-distribution profile related to dispersion DC2, undoubtedly causes narrowing of inhomogeneously broadened absorption and emission spectra, so that the intensity of the long-wavelength emission spectra of DC2 dispersion decreases. Because of the cutoff of the long-wavelength absorption spectrum of DC2 dispersion the structure of its 405-spectrum becomes more noticeable, apparently due to an additional feature of the distribution of emitting centers in DC2 over energy. The predominant intensity of the 405-peak is unchanged in both sets of spectra.

The difference in the structural inhomogeneity of dispersions raises the question of their temporal stability. Spectral analysis of their PL allows one to answer this question. Fig. 6 shows data related to dispersion DC1, but after 1.5 years (dispersion DC1*). As can be seen from Fig. 6a, in the PL spectrum DC1* there are new emitting centers, responsible for the PL in the UV region. Otherwise, 337-spectrum changes little, keeping its intensity and large width. Changes in PL spectra in the visible range are less pronounced (see Fig. 6b). Attention is drawn to high intensity of the 457-spectrum of DC1*.

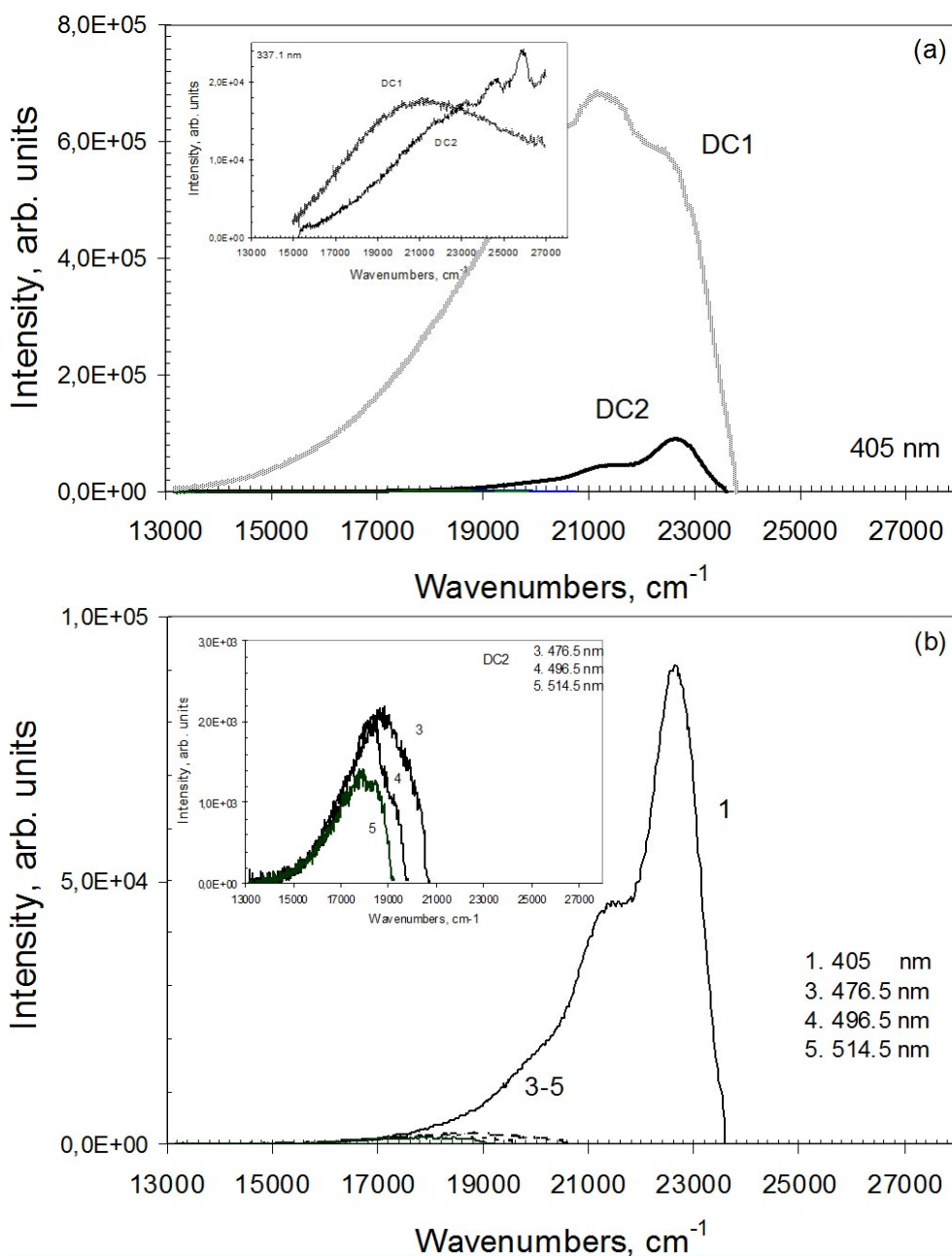


FIG. 5. Photoluminescence spectra of shungite dispersions in carbon tetrachloride at 80 K after background emission subtraction. A comparative view of 405- and 337-nm spectra (insert) of DC1 and DC2 dispersions (a); the same for spectra of DC2 dispersions at different excitations (b). Figures mark excitation wavelengths

Thus, in the low-temperature PL spectra of crystalline CTC-dispersions none of fine-structured spectra similar to Shpol'skii's spectra of organic molecules was observed. This is consistent with the absence of small particles in the size-distribution profiles of the relevant colloidal aggregates. The PL spectra are broad and overlapping with the absorption spectrum over a wide spectral range. This fact testifies to the inhomogeneous broadening of the spectra, which is the result of non-uniform distribution of the dispersions colloidal aggregates, confirmed by morphological measurements. The observed high sensitivity of PL spectra to the structural

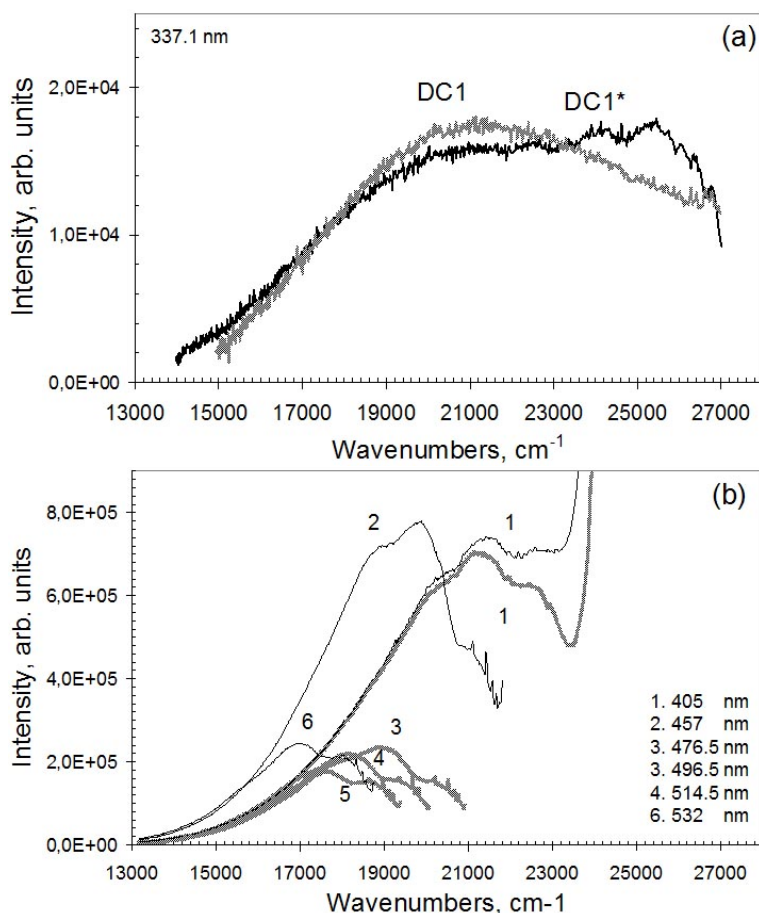


FIG. 6. Photoluminescence spectra of shungite dispersions in carbon tetrachloride at 80 K after background emission subtraction. A comparative view of 337-nm spectra (insert) of DC1 and DC1* dispersions (see text) (a); the same for spectra of DC1 (thickened curves) and DC* (thin curves) dispersions at different excitations (b). Figures mark excitation wavelengths

inhomogeneity of dispersions allows the use fluorescent spectral analysis as a method of tracking the process of the formation of primary dispersions and their aging over time. Selective excitation of emission spectra by different laser lines allows decomposition of the total spectrum into components corresponding to the excitation of different groups of emitting centers. In this case, common to all the studied dispersions is the high intensity of the emission spectra excited at λ_{exc} 405 and 457 nm.

5.2. Dispersion in Toluene

The behavior of rGO-Sh toluene dispersions is more intricate from both morphological and spectral viewpoints. Basic GQDs of aqueous dispersions are sparingly soluble in toluene, thereby resulting in toluene dispersions that are essentially colorless due to low solute concentration. In addition, the low concentration makes the dispersion very sensitive to any change in both the content and structure of dispersions. This causes structural instability of dispersions which is manifested, in particular, in the time dependence of the relevant size-distribution profiles. Thus, the three-peak distribution of the initial toluene dispersion shown in Fig. 7a, is gradually replaced by a single-peaked distribution in Fig. 7b for one to two hours. The

last distribution does not change with time and represents the distribution of the solute in the supernatant.

By analogy with carbon tetrachloride, toluene causes a drastic change in the colloidal aggregates structure thus proving once again the fractal structure of the pristine GQD colloids in the aqueous dispersions. However, if the carbon tetrachloride action can be attributed to the consolidation of the pristine colloids, the toluene results in quite an opposite effect, leading to their dispersing. Three-peak structure in Fig. 7a shows that, at the initial stage of water replacement by toluene, in resulting liquid medium there are three kinds of particles with average linear dimensions of about 2.5, 70 and 1100 nm. All three sets are characterized by a wide dispersion. Large particles are seen in the electron microscope (Fig. 7c and 7d) as freaky sprawled fragments. Over time, these three entities are replaced by one with an average size of ~ 0.25 nm. Thus, freshly produced dispersions, containing GQD aggregates of varying complexity, turns into a dispersion of individual GQDs. It should be noted that the obtained average size seems to be too small. This might be a result of the program processing the particle distribution in Zetasizer Nano ZS that is based on a spherical 3D particle approximation, whereby the output data can be assigned to the two-dimensional structural anisotropic particles with a large stretch. This makes one accept the value of 0.25 nm as very approximate and only consistent on the order of magnitude with the empirical value of ~ 1 nm for the average size of GQDs in shungite [1].

The conversion of the aqueous dispersion of aggregated GQDs into the colloidal dispersion of individual GQDs in toluene is a peculiar manifestation of the interaction of solvents with fractals described in [22]. Apparently, GQD fractals are differently ‘opaque’ or ‘transparent’ with respect to CTC and toluene, which causes a large effect. Certainly, the finding may stimulate the consideration of nanosize graphene dispersions in the framework of the fractal science similarly to the polymer study [22]. As for the graphene photonics, the obtained toluene dispersion has allowed the investigation of individual GQDs for the first time.

Figure 8 shows the PL spectra of colloidal dispersions for individual GQDs in toluene. The *brutto* experimental spectra, each of which is a superposition of the Raman spectrum of toluene and PL spectrum of the dispersion, are presented in Fig. 8a. Note the clearly visible enhancement of Raman scattering of toluene from $20000 - 17000$ cm^{-1} . Fig. 8b shows the PL spectra after subtracting Raman spectra. The spectra presented in the figure can be divided into three groups. The first group includes the 337-spectrum (7) that in the UV region is the PL spectrum, similar in shape to the UV PL spectrum of toluene, but shifted to longer wavelengths. This part of the spectrum should apparently be attributed to the PL of some impurities in toluene. The main contribution into the PL 337-spectrum from $24000 - 17000$ cm^{-1} is associated with the emission of all GQDs available in the dispersion. This spectrum is broad and structureless, which apparently indicates the structural inhomogeneity of the GQD colloids.

PL 405- and 476-spectra (1 and 3 from $23000 - 17000$ cm^{-1} should be attributed to the second group. Both spectra have clearly defined structure that is most clearly expressed in the 405-spectrum. The spectrum is characteristic of a complex molecule with allowed electronic transitions. Assuming that the maximum frequency at 22910 cm^{-1} determines the position of pure electronic transition, the longer wavelength doublet at $\sim 21560 - 21330$ cm^{-1} can be interpreted as vibronic transitions. The distance between the doublet peaks and the pure electronic band constitutes $1350 - 1580$ cm^{-1} that is consistent with the frequencies of totally symmetric vibrations of C–C graphene skeleton, commonly observed in the Raman spectra. Similarly, two peaks of the much lower intensity 476-spectrum, which are wider than in the previous case, are divided by the average frequency of 1490 cm^{-1} . PL 457-spectrum, shown in Fig. 8c (curve 2) is similar to spectra 1 and 3, in intensity closer to the 405-spectrum. All

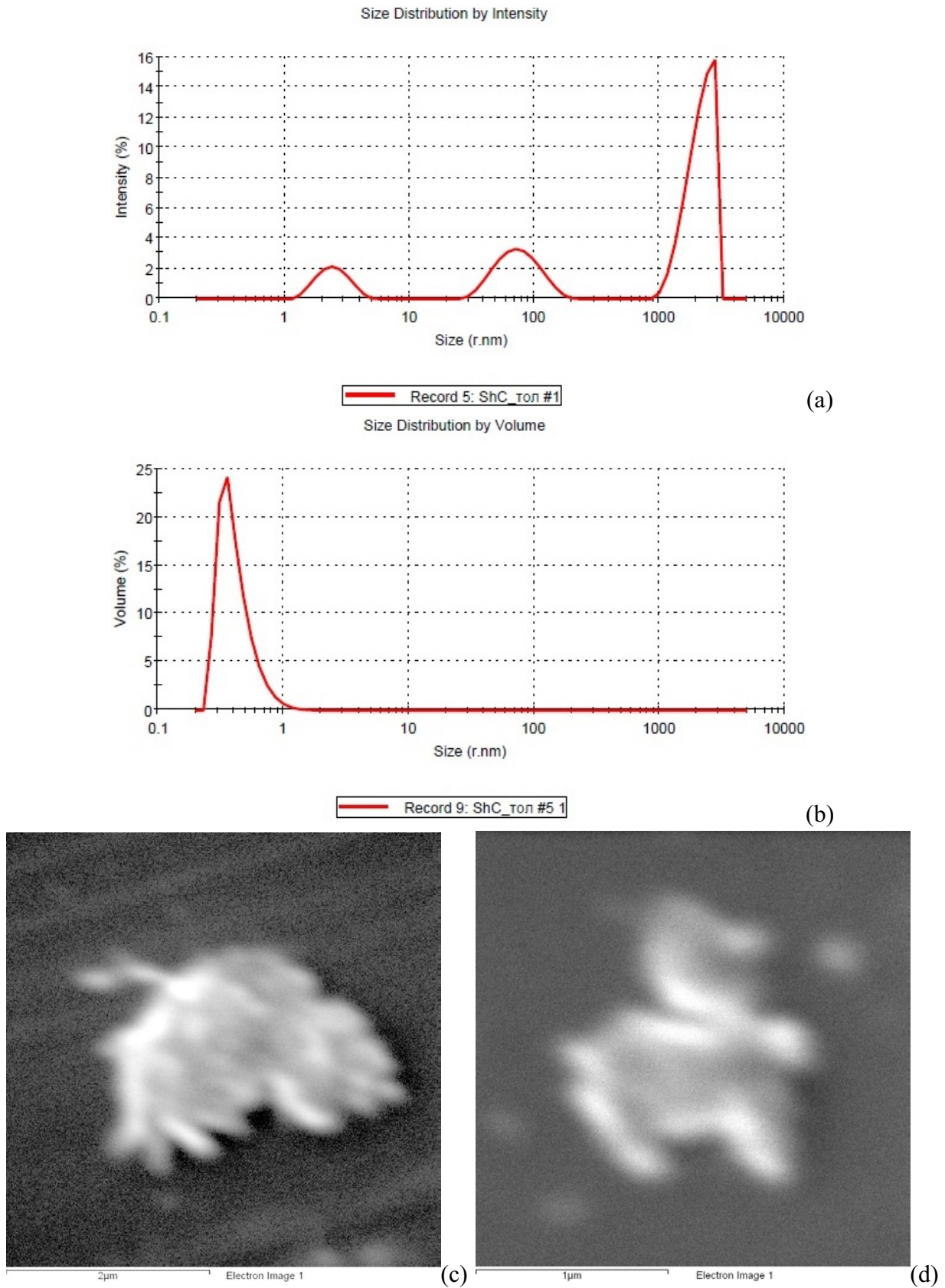


FIG. 7. Size-distribution profiles of colloidal aggregates in shungite toluene dispersion (a and b) (see text) and SEM images of the dispersion condensates on glass substrate (c) and (d): Scale bar $2 \mu\text{m}$ and $1 \mu\text{m}$, respectively. Carbon concentrations constitute 0.08 (a) and 0.04 (b) mg/ml

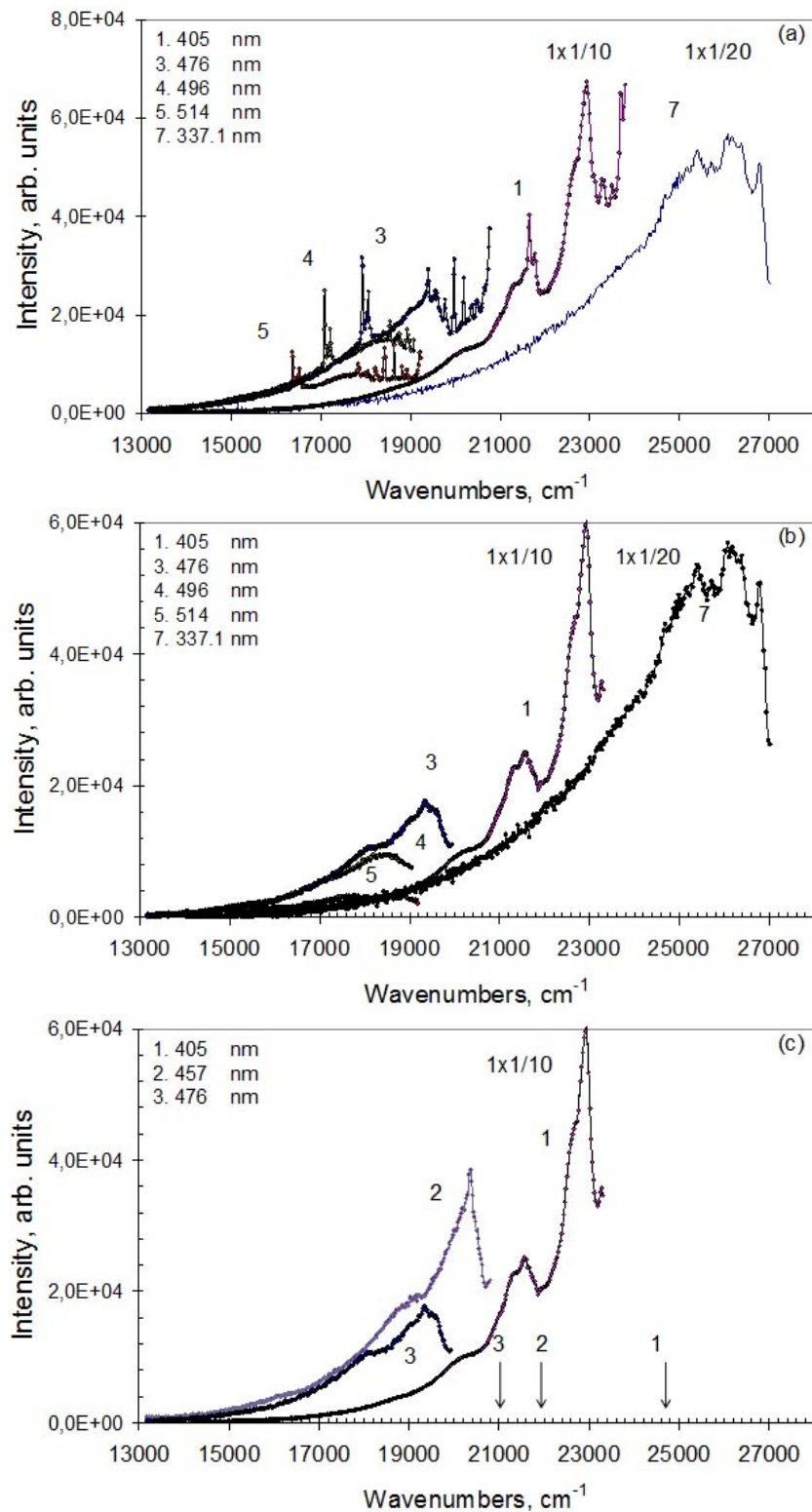


FIG. 8. Photoluminescence spectra of shungite toluene dispersion at 80 K as observed (a), after subtraction of Raman scattering of toluene (b), and attributed to individual GQDs only (c). Figures and arrows mark excitation wavelengths

three spectra are related to individual rGO fragments, albeit of different size that increases when going from 405-spectrum to 457- and 476-spectrum.

The shape of 496- and 514-spectrum substantially differs from that of the second group spectra. Instead of the two peaks, a broad band is observed in both cases. This feature makes these spectra attributable to the third group and associate them with the appearance of not individual frozen GQDs but with their possible clusters (such as, say, dimeric homo- (GQD+GQD) and hetero- (GQD+toluene) structured charge transfer complexes and so forth). The evidence of such a possibility will be discussed in the next section.

The conducted spectral studies of the rGO-Sh toluene dispersions confirmed once again the status of toluene as a good solvent and a good crystalline matrix, which allows for obtaining structured spectra of individual complex molecules under conditions when in other solvents the molecules form fractals. This ability of toluene allowed for the first time to get the spectra of both individual GQDs and their small clusters. The finding represents the first reliable empirical basis for further theoretical treatment of the spectra observed. Simultaneously with this, use of toluene and carbon tetrachloride as solvents convincingly showed a strong tendency of nanoscale graphenes to form fractals, which should be taken into account in practical applications.

6. Discussion

As follows from the results presented in the previous sections, rGO-Sh dispersions are colloidal dispersions regardless of the solvent, whether water, carbon tetrachloride or toluene. The dispersion colloid's structure depends on the solvent and thereafter is substantially different. This issue deserves a special investigation. Thus, the replacement of water with carbon tetrachloride leads to multiple enlargement of the pristine colloids which promotes the formation of a quasi-crystalline image of the condensate structure. At present, the colloid's detailed structure remains unclear. In contrast to carbon tetrachloride, toluene causes the decomposition of pristine colloids into individual rGO fragments. The last facts cast doubt on a direct link between the structure of the dispersions fractals and the elements of fractal structure of solid shungite or its post-treated condensate. The observed solvent-stimulated structural transformation is a consequence of the geometric peculiarities of fractals behavior in liquids [22]. The resulting spectral data can be the basis for further study of this effect.

The spectral behavior of the aqueous and CTC-dispersions with large colloids is quite similar, despite the significant difference in size and structure of the latter. Moreover, the features of the PL spectra of these dispersions practically replicate patterns that are typical for the aqueous rGO-Sy dispersions discussed in detail in Section 1. This allows one to conclude that one and the same structural element of the colloidal aggregates of both rGO-Sh and rGO-Sy dispersions is responsible for the emission in spite of pronounced morphological difference of its packing in all these cases. According to the modern view of the shungite structure [1] and a common opinion on the origin of synthetic GQDs [11, 12], nanosize rGO fragments should play a role thus representing GQDs of the rGO colloidal dispersions in all these cases.

Specific effects of toluene, which caused the decomposition of pristine particles into individual rGO fragments with succeeding embedding of them into a crystalline matrix of toluene, allowed us for the first time to obtain the PL spectrum of individual rGO fragments. Obviously, resulting fragments are of different size and shape, which determines the structural inhomogeneity of toluene dispersions. This feature of toluene dispersions is common with the other dispersions and explains the dependence of PL spectra on λ_{exc} that is the main spectral feature of GQDs, both synthetic [11, 12] and of shungite origin.

The structural inhomogeneity of GQDs colloidal dispersions is mainly a result of two causes, namely, internal and external. The internal cause concerns the uncertainty in the structure

(size and shape) of the basic rGO fragments. It is the most significant for shungite while, under laboratory conditions, the rGO fragments' structure might be more standardized [11, 12]. Nanosize rGO basic structural elements of solid shungite are formed under the conditions of a serious competition of different processes [1], among which the most valuable are: 1) natural graphitization of carbon sediments, accompanied by a simultaneous oxidation of the graphene fragments and their reduction in water vapor; 2) the retention of water molecules in space between fragments and removal of the water molecules from the space into the environment, and 3) the multilevel aggregation of rGO fragments providing the formation of a monolithic fractal structure. Naturally, that achieved balance between the kinetically-different-factors is significantly influenced by random effects, so that the rGO fragments of natural shungite, which were created via natural processes, are statistically averaged over a wide range of fragments that differ in size, shape, and chemical composition. Obviously, the reverse procedure of the shungite dispersion in water is statistically also nonuniform with respect to colloidal aggregates, so that there is a strong dependence of the dispersions on the technological protocol, which results in a change in the dispersion composition caused by slight protocol variations.

The external cause is due to the fractal structure of colloidal aggregates. The fractals themselves are highly inhomogeneous, moreover, they strongly depend upon the solvent. These two reasons determine the feature of the GQD spectra in aqueous and CTC-dispersions, while the first one dominates in the case of toluene dispersions. The same two reasons lay the foundation for the main feature of GQDs spectra, explaining their positions by the energy, on the one hand, and large broadening, on the other.

The structural PL spectra allow one to pose the question about identifying the interaction effect of dissolved rGO fragments with each other and with the solvent. Nanosize rGO fragments have high donor-and-acceptor properties (low ionization potential and high electron affinity) and can exhibit both donor and acceptor properties, so that clusters of fragments (dimers, trimers, and so forth) are typical charge transfer complexes. Besides this, toluene is a good electron donor, due to which it can form a charge-transfer complex with any rGO fragment, which acts as an electron acceptor. The energy spectrum of the complex electron-hole states, which depends on the distance between the molecules, on the initial parameters, is similar to the electron-hole spectrum of fullerenes C_{60} clusters themselves and with toluene [19], positioned in the $17000 - 20000 \text{ cm}^{-1}$ region. By analogy, with fullerene C_{60} solutions [19], the enhancement of the Raman spectrum of toluene is due to superposition of the spectrum over that one of electron-hole states, in accordance with the theory of light amplification caused by nonlinear optical phenomena [28]. Additionally, the formation of rGO-toluene charge transfer complexes may promote the formation of stable chemical composites during photochemical reactions [29] that might be responsible for the PL spectra of the third group that were observed in toluene dispersions. Certainly, this assumption requires further theoretical and experimental investigation.

7. Conclusion

The photonics of shungite colloidal dispersions faces the problem that the large statistical inhomogeneity inherent in the quantum dot as an object of the study makes it difficult to interpret the results in detail. Consequently, common patterns that are observed on the background of this inhomogeneity become most important. In the case of the considered dispersions, the common patterns include, primarily, the dispersion PL in the visible region, which is characteristic for large molecules consisting of fused benzenoid rings. This made it possible to confirm the earlier findings that graphene-like structures of limited size, namely, rGO fragments are the basic structural elements for all the dispersions. The second feature concerns the dependence

of the position and intensity of selective PL spectra on the exciting light wavelength λ_{exc} . This feature lies in the fact that regardless of the composition and solvent of dispersions, the PL excitation at λ_{exc} 405 and 457 nm provides the highest PL intensity while excitation at either longer or shorter wavelengths produces a much lesser intensity of the emission. The answer to this question must be sought in the calculated absorption and photoluminescence spectra of graphene quantum dots, which we attributed to nanosize fragments of reduced graphene.

Acknowledgments

A financial support provided by the Ministry of Science and High Education of the Russian Federation grant 2.8223.2013, Basic Research Program, RAS, Earth Sciences Section-5, and grant RFBI 13-03-00422 is highly acknowledged.

References

- [1] Rozhkova N.N., Sheka E.F. Shungite as loosely packed fractal nets of graphene-based quantum dots. arXiv:1308.0794 [cond-mat.mtrl-sci] (2013).
- [2] Trauzettel B., Bulaev D.V., Loss D., Burkard G. Spin qubits in graphene quantum dots. *Nat. Phys.*, **3**, P. 192–196 (2007).
- [3] Guclu A., Potasz P., Hawrylak P. Electric-field controlled pin in bilayer triangular graphene quantum dots. *Phys. Rev. B*, **84**, P. 035425 (2011).
- [4] Ritter K.A., Lyding J.W. The influence of edge structure on the electronic properties of graphene quantum dots and nanoribbons. *Nat. Mater.*, **8**, P. 235–242 (2009).
- [5] Pan D., Zhang J., Li Z., Wu M. Hydrothermal route for cutting graphene sheets into blue-luminescent graphene quantum dots. *Adv. Mater.*, **22**, P. 734–738 (2010).
- [6] Shen J., Zhu Y., et al. Facile preparation and upconversion luminescence of graphene quantum dots. *Chem. Commun.*, **47**, P. 2580–2582 (2011).
- [7] Zhang Z.Z., Chang K. Tuning of energy levels and optical properties of graphene quantum dots. *Phys. Rev. B*, **77**, P. 235411 (2008).
- [8] Gupta V., Chaudhary N., et al. Luminescent graphene quantum dots for organic photovoltaic devices. *J. Am. Chem. Soc.*, **133**, P. 9960–9963 (2011).
- [9] Liu R., Wu D., Feng X., Mullen K. Bottom-up fabrication of photoluminescent graphene quantum dots with uniform morphology. *J. Am. Chem. Soc.*, **133**, P. 15221–15223 (2011).
- [10] Yan X., Li B., Li L.-S. Colloidal graphene quantum dots with well-defined structures. *Acc. Chem. Res.*, DOI: 10.1021/ar300137p.
- [11] Tang L., Ji R., et al. Deep ultraviolet photoluminescence of water-soluble self-passivated graphene quantum dots. *ACS Nano*, **6**, P. 5102–5110 (2012).
- [12] Li L., Wu G., et al. Focusing on luminescent graphene quantum dots: current status and future perspectives. *Nanoscale*, **5**, P. 4015–4039 (2013).
- [13] Zhou X., Zhang Y., et al. Photo-Fenton reaction of graphene oxide: A new strategy to prepare graphene quantum dots for DNA cleavage. *ACS Nano*, **6**, P. 6592–6599 (2012).
- [14] Dong Y., Chen C., et al. One-step and high yield simultaneous preparation of single- and multi-layer graphene quantum dots from CX-72 carbon black. *J. Mater. Chem.*, **22**, P. 8764–8766 (2012).
- [15] M. Zhang, L. Bai, et al. Facile synthesis of water-soluble, highly fluorescent graphene quantum dots as a robust biological label for stem cells. *J. Mater. Chem.*, **22**, P. 7461–7467 (2012).
- [16] Lin L., Zhang S. Creating high yield water soluble luminescent graphene quantum dots via exfoliating and disintegrating carbon nanotubes and graphite flakes. *Chem. Commun.*, **48**, P. 10177–10179 (2012).
- [17] Chen S., Liu J.-W., et al. Unusual emission transformation of graphene quantum dots induced by self-assembled aggregation. *Chem. Commun.*, **48**, P. 7637–7639 (2012).
- [18] Razbirin B.S., Sheka E.F., et al. Enhanced Raman scattering provided by fullerene nanoclusters. *JETP Lett.*, **87**, P. 133–139 (2008).
- [19] Razbirin B.S., Sheka E.F., et al. The nature of enhanced linear and nonlinear optical effects in fullerenes in solution. *JETP*, **108**, P. 738–750 (2009).
- [20] Razbirin B.S., Sheka E.F., et al. Shpol'ski effect in optical spectra of frozen solutions. *Phys. Sol. State*, **51**, P. 1315–1319 (2009).

- [21] Sheka E.F., Razbirin B.S., et al. Fullerene-cluster amplifiers and nanophotonics of fullerene solutions. *J. Nanophoton.*, **3**, P. 033501 (2009).
- [22] Witten T.A. Polymer solutions: A geometric introduction. In *Soft Matter Physics*. Eds. M. Daoud and C.E. Williams. Springer-Verlag, Berlin Heidelberg, 1999, P. 261–288.
- [23] Gouyet J.-F. *Physics and Fractal Structures*. Masson Springer: Paris/New York, 1996.
- [24] Park S., An J., et al. Colloidal suspensions of highly reduced graphene oxide in a wide variety of organic solvents. *Nano Lett.*, **9**, P. 1593–1597 (2009).
- [25] Hamilton C.E., Lomeda J.R., et al. High-yield organic dispersions of unfunctionalized graphene. *Nano Lett.*, **9**, P. 3460–3462 (2009).
- [26] Rozhkova N.N., Yemel'yanova G.I., et al. From stable aqueous dispersion of carbon nanoparticles to the clusters of metastable shungite carbon. *Glass Phys. Chem.*, **37**, P. 613–618 (2011).
- [27] Shpol'skii E.V. New data on the nature of the quasilinear spectra of organic compounds. *Phys.-Uspekhi*, **6**, P. 411–427 (1963).
- [28] Heritage J.P., Glass A.M. Nonlinear optical effects. In *Surface Enhanced Raman Scattering*. Eds. R.K.Chang and F.E.Furtak. NY and London: Plenum Press. 1982, P. 391–412.
- [29] Sheka E.F. Nanophotonics of fullerene. 1. Chemistry and medicine. *Nanosci. Nanotechn. Lett.*, **3**, P. 28–33 (2011).